analytical chemistry

pubs.acs.org/ac Article

Dumbbell Hybridization Chain Reaction Based Electrochemical Biosensor for Ultrasensitive Detection of Exosomal miRNA

Peng Miao* and Yuguo Tang

Cite This: *Anal. Chem.* 2020, 92, 12026−12032 Read Online

ACCESS | Metrics & More | Article Recommendations | Supporting Information

ABSTRACT: Exosomal miRNA is an ideal source of noninvasive biomarker for the diagnosis of cancer. Sensitive and accurate analysis of exosomal miRNA plays an important role in facilitating clinical applications. Herein, we have developed a novel electrochemical method for exosomal miRNA assay coupling strand displacement amplification (SDA) and dumbbell hybridization chain reaction (DHCR). The target triggered isothermal SDA process generates a large number of single-stranded DNA products to assist the formation of the three-way junction structure on the electrode surface. In addition, dumbbell DNA fuel strands (DHP1 and DHP2) are designed for the hybridization chain reaction. This novel form of HCR produces DNA nanostructures with a tight conformation, which facilitates the enhancement of the electrochemical response. The combination of the dual signal amplification significantly improves the sensitivity for the exosomal miRNA assay, resulting in a limit of detection (LOD) as low as 7.3 aM. More importantly, the method is successfully applied in the analysis of cells and human serum samples, which demonstrates the potential utility in point-of-care testing (POCT) applications.

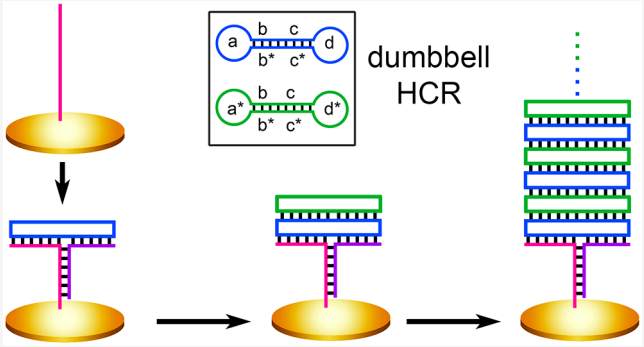

The miRNAs are a class of endogenous noncoding RNAs with short single-stranded sequences.[1] miRNA is able to specifically hybridize with corresponding mRNA and negatively regulate gene transcription.[2] Numerous studies have shown the expression profiles of miRNAs are closely associated with human diseases including infectious diseases, diabetes neurodegenerative diseases, and cancers.[3−5] Thus, miRNAs have been employed as promising candidates of biomarkers for the disease diagnosis.[6] miRNA can be stably present in serum or plasma conditions. Moreover, compared with plasma derived circulating miRNA, extracellular vesicle derived miRNA shows more merits as a biomarker. First, extracellular vesicles enrich miRNA, and the detection of higher abundant miRNA is easier and more reliable;[7] second, the protection by extracellular vesicles helps the resistance of RNase degradation;[8] third, the stability of the miRNA sample is further enhanced, which can be used even after being treated with multiple freeze−thaw cycles or extreme pH conditions.[9] Exosomes are a kind of nanoscale extracellular vesicles with sizes ranging from 30 to 150 nm.[10] They transfer exosomal cargoes (DNA, RNA, proteins, etc.) from donor to recipient cells.[11] Thus, the analysis of exosomal miRNAs has attracted much attention with extraordinary diagnostic values.[12,13] Nevertheless, it remains a formidable challenge to quantify miRNA conveniently, which is due to the inherent properties of miRNA including short length, high sequence homology, and low abundance.[14]

Quantitative reverse transcription-polymerase chain reaction (qRT-PCR) is the standard protocol for the quantification of RNAs.[15] Microarrays and Northern blotting are another two commonly used methods.[16] However, these techniques suffer limitations like time-consuming procedures, large sample volumes, complicated primer designs, and sophisticated instruments, which hamper their wide applications in the point-of-care testing (POCT) area. Recently, many novel sensing strategies have been proposed. For instance, Liu et al. integrated the duplex-specific nuclease assisted recycling process and strand displacement reaction for ultrasensitive detection of miRNA.[17] Both of the reactions in tandem are isothermal. Especially, strand displacement amplification (SDA) is quite competitive in POCT applications with mild reaction conditions and high amplification efficiency.[18] Hybridization chain reaction (HCR) is another efficient isothermal signal amplification protocol, which has been widely applied.[19] It is even simpler without the involvement of enzymes.[20] The basic form is linear elongation of nicked double-stranded DNA with single-stranded initiator DNA and

Received: June 21, 2020
Accepted: July 27, 2020
Published: July 27, 2020

https://dx.doi.org/10.1021/acs.analchem.0c02654
Anal. Chem. 2020, 92, 12026−12032

two hairpin fuel DNAs.[21] Since signal amplification performance is also related to the morphology of nanostructured DNA products, HCR can be further modified or improved.[22]

In this work, we have developed an improved HCR form, dumbbell hybridization chain reaction (DHCR), which replaces traditional hairpin structured fuel strands by dumbbell structured DNA probes. More tight DNA nanostructures can be produced, which has the potential to enhance signal intensity. On the other hand, target exosomal miRNA triggered SDA is first carried out to generate a large number of single-stranded DNA products. DNA junction structures are formed to link SDA and DHCR, which helps the immobilization of a large number of electrochemical species on the surface of the electrode.[23] When one analyzes the electrochemical response, the initial miRNA level can be evaluated. Experimental results demonstrate ultrahigh sensitivity, and the proposed method is applicable in exosomal miRNA from both cultured cells and clinical cancer patients' serums.

EXPERIMENTAL SECTION

Chemicals and Instruments. Sodium dihydrogen phosphate (NaH_2PO_4), dibasic sodium phosphate (Na_2HPO_4), sodium chloride (NaCl), tris (2-carboxyethyl) phosphine (TCEP), diethypyrocarbonate (DEPC), mercaptohexanol (MCH), and ethylenediaminetetraacetic acid (EDTA) were purchased from Sigma (USA). T4 DNA ligase, Klenow fragment polymerase, Nb.BbvCI nicking endonuclease (NEase), dNTPs, and CutSmart buffer were purchased from New England Biolabs (Beijing, China). Dulbecco's Modified Eagle Medium (DMEM) and fetal bovine serum (FBS) were from Beijing Solarbio Science & Technology Co., Ltd. (Beijing, China). All other chemicals were of analytical grade without further purification. DNA/RNA and 20 bp DNA Ladder were ordered from Takara Biotechnology Co., Ltd. (Dalian, China). Detailed sequences and modifications were listed in Table S1. HeLa, 293, A549, and MCF-10A cells were from the Institute of Biochemistry and Cell Biology, Chinese Academy of Sciences (Shanghai, China). Human serum samples were collected from a local hospital (Suzhou, China). The qRT-PCR kit was purchased from Tiangen Biotech Co., Ltd. (Beijing, China). The TRIzol total RNA isolation kit was ordered from Sangon Biotechnology Co. Ltd. (Shanghai, China). Water used to prepare all solutions was previously purified by a Millipore water purification system (with a specific resistance of 18 MΩ·cm) and then treated with DEPC.

Transmission electron microscopic (TEM) images were taken by a FEI Tecnai G20 transmission electron microscopy (FEI, USA). Polyacrylamide gel images were taken under UV light by a GelDoc XR$^+$ System (Bio-Rad, USA). Exosomes were isolated by the use of an Ultracentrifuge Optima L-100XP (Beckman Coulter, USA). The diameter and concentration of exosomes were determined by a NanoSight LM10 (Malvern Instruments, UK). qRT-PCR experiments were performed on an ABI 7500 Real-Time PCR System (ABI Life Technologies, USA). All electrochemical measurements were carried out by a CHI 660D electrochemical workstation (CH Instruments, China).

Cell Culture and Exosomal RNA Extraction. All cells were cultured in DMEM spiked with 10% FBS at 37 °C in a 5% CO_2 atmosphere. After reaching the exponential growth period, the cells were washed for three times with PBS, which were then incubated with FBS-free DMEM for 48 h. Afterward, the culture supernatants were collected for the isolation of exosomes by ultracentrifugation. Briefly, the supernatants were first centrifuged at 2000*g* for 0.5 h and then at 10 000*g* for another 0.5 h in order to eliminate cells and proteins. Subsequently, a further centrifugation at 110 000*g* for 2 h was carried out. The precipitated exosome sediments were then resuspended in 1 mL of PBS. Total RNAs were then extracted from the collected exosomes by using the TRIzol total RNA isolation kit with standard manipulation.

Strand Displacement Amplification. Standard miRNA samples with a series of concentrations were prepared. Next, they were blended with 2 μM template (20 mM Tris-acetate, 10 mM magnesium acetate, 50 mM potassium acetate, 100 μg mL^{-1} BSA, pH 7.9) containing 100 μM dNTPs, 0.1 unit μL^{-1} Nb.BbvCI, and 0.04 unit μL^{-1} Klenow fragment polymerase. The SDA reaction was conducted at 30 °C for 1 h, followed by the termination of heating to 85 °C for 20 min.

Preparation of DNA Modified Electrode. The gold working electrode was first treated with piranha solution (*Caution: highly corrosive*) for 5 min. Then, it was rinsed carefully with pure water before being polished with silicon carbide paper (P5000) and alumina powders (1.0, 0.3, 0.05 μm), successively. After that, the electrode was sonicated in ethanol and double-distilled water, each for 5 min. Next, it was immersed in nitric acid (50%) for 0.5 h and then electrochemically cleaned with 0.5 M H_2SO_4. The pretreated electrode was rinsed again and incubated with 0.5 μM TWJ1 (10 mM Tris-HCl, 1 mM EDTA, 10 mM TCEP, 0.1 M NaCl, pH 7.4) for 8 h, followed by the treatment with 1 mM MCH for 0.5 h.

Preparation of Circular Dumbbell DNAs and DHCR. Circular dumbbell DNA fuel strands (DHP1 and DHP2) were prepared from their 5′-phosphorylated precursors catalyzed by T4 DNA ligase. Briefly, 10 μL of DHP1 or DHP2 (10 μM) was mixed with 5 μL of 10× T4 DNA ligase buffer, 3 μL of T4 DNA ligase (200 unit μL^{-1}), and 32 μL of DEPC treated pure water. The mixture was placed in an incubator with a temperature of 16 °C for 5 h. After that, the reaction was terminated by heating to 65 °C for 10 min. The SDA product was then mixed with the two ligation product with a volume ratio of 1:1:1. The TWJ1 modified electrode was then immersed in the above solution for 100 min at room temperature before electrochemical measurements.

Electrochemical Measurements. The traditional three-electrode system was applied in this work. Briefly, a saturated calomel reference electrode, a platinum wire counter electrode, and a DNA modified gold working electrode were assembled. In order to investigate the electrochemical properties of the working electrode during different reaction periods, cyclic voltammetry (CV) and electrochemical impedance spectroscopy (EIS) were carried out with the electrolyte (5 mM $[Fe(CN)_6]^{3-/4-}$, 1 M KNO_3). CV was scanned from +0.7 V to −0.1 V with a rate of 50 mV s^{-1}. EIS was conducted upon the application of 0.205 V biasing potential and 5 mV amplitude in the frequency range of 0.1 Hz to 100 kHz. To quantify exosomal miRNA, square wave voltammetry (SWV) was performed in the electrolyte (20 mM Tris-HCl, 50 μM TCEP, 100 mM NaCl, 50 mM $MgCl_2$, pH 7.4). The scan range and rate were −0.02 to −0.55 V and 50 mV s^{-1}, respectively. The step potential was 4 mV, and the frequency was set to 70 Hz.

RESULTS AND DISCUSSION

Sensing Principle. The detailed working mechanism of the DHCR based electrochemical biosensor is illustrated in

https://dx.doi.org/10.1021/acs.analchem.0c02654
Anal. Chem. 2020, 92, 12026−12032

Scheme 1. The sensing approach contains two parts. Part one is target miRNA initiated strand displacement amplification in

Scheme 1. Illustration of the DHCR Based Biosensor for the Exosomal miRNA Assay

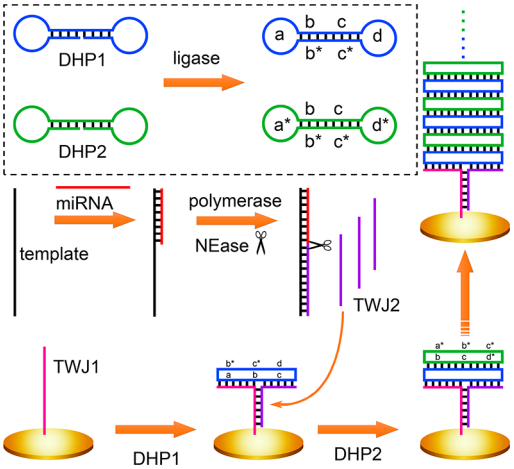

the solution. miRNA hybridizes with template DNA, and the extension reaction is catalyzed by polymerase to form the complete duplex. A nick is then created by NEase. With the continued extension reaction, single-stranded TWJ2 is displaced. Due to the recycled nicking and extension reactions, a large number of TWJ2 strands are generated, which are essential for the following formation of the three-way junction structure. On the other hand, part two of the sensing approach is the dumbbell hybridization chain reaction on the electrode interface. Two single-stranded DNA probes are designed: DHP1 contains six segments of b*, a, b, c, d, and c* (from 5′ to 3′), while DHP2 contains six segments of b*, a*, b, c, d*, and c* (from to 5′ to 3′). Due to the complementary sequences (b/b*; c/c*), dumbbell structures can be formed. In addition, with 5′ phosphorylated ends, DHP1 and -2 are transformed into closed states catalyzed by T4 DNA ligase. Initially, the two self-complementary dumbbell structures are sufficiently stable.[24] However, the three-way junction can be formed between DHP1 and TWJ1 on the electrode and TWJ2 generated by SDA. In this period, the toehold part of DHP1 (segment a) is first recognized and branch migration occurs, which gradually opens the dumbbell structure until the formation of a complete three-way junction. The standard free energy variation (ΔG) for the activation of DHP1 (from dumbbell to open state) is calculated to be −12.39 kJ mol^{-1}, indicating the tendency of the reaction. In addition, the single-stranded part of DHP1 can be further used to active the dumbbell structure of DHP2 in a similar way. ΔG for the total reaction is calculated to be −29.08 kJ mol^{-1}. The more negative value demonstrates an easier assembly process (Figure S1A). After stacking of DHP2 on DHP1, the free single-stranded part of DHP2 in turn activates the dumbbell structure of a new DHP1. The recycled hybridization reactions leads to tight assembly of DHP1 and DHP2 in succession. After recording the electrochemical signals labeled at the 3′ end of DHP1, the initial target miRNA level can be evaluated. To make sure only DHCR can be triggered in the presence of target, we have calculated ΔG for self-assembly between DHP1 and -2 without the three-way junction, which is +5.7 kJ mol^{-1} (Figure S1B). The positive value indicates DHP1 and -2 will maintain dumbbell structures without any input strands.

Feasibility Confirmation and Electrochemical Characterization. The successful SDA is first identified by polyacrylamide gel electrophoresis (PAGE). In Figure S2A, lanes a to c show the bands of miRNA, template, and their hybrid, respectively. DNA with larger molecule weight runs slower in the gel; thus, the position is higher. As expected, after the interaction between target and template, the partial duplex is located in the higher position in the gel. Meanwhile, the introduction of polymerase helps the extension reaction and results in the completed duplex. Thus, the band is getting higher (lane d). On the other hand, with the further employment of NEase, a large number of TWJ2 strands are produced (lane e), which is reflected by the lower band in the gel (Figure S2A). DHCR is also confirmed by PAGE. In Figure S2B, lanes a to c show the bands of TWJ1, DHP1 and -2, respectively. After mixing TWJ1 and DHP1, no new band appears, demonstrating that TWJ1 and DHP1 cannot hybridize with each other directly (lane d). However, after the introduction of TWJ2, a three-way junction forms, which is confirmed by the new band with a higher position in the gel (lane e). In addition, after further introduction of DHP2, another new band with even a higher position is observed (lane f), which is the DHCR product with a large molecular weight (Figure S2B).

We have then carried out CV, EIS, and SWV techniques to probe the electrochemical properties during different reaction steps. As shown in Figure 1A, a pair of well-defined current

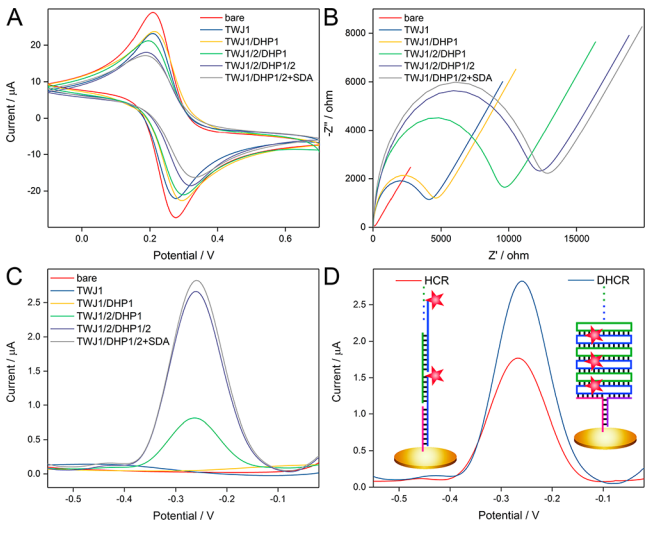

Figure 1. (A) Cyclic voltammograms, (B) Nyquist diagrams, and (C) square wave voltammograms of bare electrode, TWJ1 modified electrode, and TWJ1 modified electrode after incubation with DHP1, TWJ2 and DHP1, TWJ2 and DHP1/2, and DHP1/2 with SDA product, respectively. (D) Square wave voltammogram responses of linear HCR and DHCR.

peaks is shown for the bare gold electrode. After being modified with TWJ1, the peak currents drop, which is due to the repellent between negatively charged DNA and [Fe(CN)$_6$]$^{3-/4-}$. Next, we have immersed TWJ1 modified electrode in DHP1. However, the recorded peak currents are nearly the same as those of the TWJ1 modified electrode, which reflects that TWJ1 cannot interact with DHP1 directly. Only in the presence of TWJ2, a three-way junction is formed

https://dx.doi.org/10.1021/acs.analchem.0c02654
Anal. Chem. 2020, 92, 12026−12032

(TWJ1, -2, and DHP1) and the peak currents decrease due to the more negative interface. DHP2 is then added, and DHCR is achieved, demonstrated by the further decreased peak currents. In addition, we have replaced the directly added TWJ2 with target initiated SDA product. Since the reaction also generates a large number of TWJ2, the CV peaks are also decreased compared with the TWJ1/2/DHP1 case. EIS results are then measured and summarized in Figure 1B. In a typical Nyquist plot, the diameter of the semicircle domain is the reflection of electron transfer resistance. No semicircle domain is observed for the bare electrode, indicating an excellent electron transfer rate of the substrate gold electrode. After being modified with TWJ1, the negatively charged DNA molecules repel $[Fe(CN)_6]^{3-/4-}$, resulting in a significant charge transfer resistance (R_{ct}) of 3672 Ω. After further incubation with DHP1, no efficient hybridization occurs and the diameter of the semicircle domain is nearly the same as that with the TWJ1 modified electrode. The slightly increased R_{ct} of 3851 Ω is due to nonspecific physical adsorption. On the contrary, after the formation of the three-way junction (TWJ1/2/DHP1) on the electrode surface, the interface becomes much more negative to repel $[Fe(CN)_6]^{3-/4-}$. As a result, the diameter of the semicircle increases and R_{ct} is increased to 7952 Ω. After further addition of DHP2, the formed DHCR product leads to an even larger semicircle domain with R_{ct} of 11 839 Ω. Moreover, we have tried to provide TWJ2 by target miRNA initiated SDA. DHCR can also be achieved, and a similarly large R_{ct} of 12 204 Ω is observed. The EIS results are well consistent with the CV results. Since we have labeled MB on the end of DHP1, we can record SWV curves to study the immobilization of DHP1 on the electrode (Figure 1C). Noncovalent MB has been widely used as an electrochemical reporter for DNA electrochemistry. It also has additional merit in that it undergoes electrocatalytic signal amplification. Herein, we have applied covalent tethering MB to promise its restricted mobility and address the stringent requirement for the high quality DNA layer. Without the localization of DHP1, flat SWV curves are obtained. The three-way junction helps the immobilization of the DHP1 layer; thus, a significant current peak (0.81 μA) appears (TWJ1/2/DHP1). We have then supplied DHP2 in the system for DHCR, the process of which helps loading of more DHP1 on the electrode; thus, the peak intensity is further enhanced to be 2.66 μA. Moreover, we eliminate the direct addition of TWJ2. Instead, target miRNA initiated SDA is conducted to generate this essential strand for three-way junction formation. After further addition of DHP1 and -2, another sharp current peak is achieved (2.82 μA), which is comparable with the case of TWJ1/2/DHP1/2. We have then compared the performances of common linear HCR (using H0, H1, and H2) and DHCR in this electrochemical system (Figure 1D). Although the concentrations of trigger and fuel strands are the same, the SWV peak of DHCR is much larger than that of traditional HCR (2.82 μA versus 1.77 μA). The reason is that distance between MB on the linear HCR product is relatively much larger. On the contrary, the DHCR product contains a more tight conformation, which benefits the enrichment of more MB near the electrode surface. The higher steric hindrance of the DHCR product might not significantly influence the electrochemical response of MB due to excellent DNA-mediated charge transport.

Experimental Optimization and Quantification of miRNA. To achieve the best analytical performance of the electrochemical method, we have optimized several key conditions. The density of TWJ1 should be well controlled since larger density may be unfavorable for effective hybridization. A larger amount of enzymes can improve the efficiency of SDA. Nevertheless, the cost must be considered and less enzyme usage is better. The reaction times of SDA and DHCR should also be shortened to improve the practical utility. After comparing the SWV peaks, we have achieved the following conditions: 0.5 μM, 0.1 unit μL^{-1}, and 60 and 100 min, respectively (Figure S3). Under these optimized conditions, we have explored the quantitative performance of miRNA by recording corresponding SWV curves. As shown in Figure 2A,

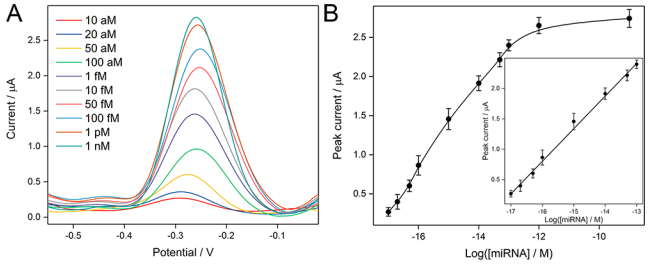

Figure 2. (A) Square wave voltammograms for the detection of miRNA with the concentrations of 10^{-17}, 2×10^{-17}, 5×10^{-17}, 10^{-16}, 10^{-15}, 10^{-14}, 5×10^{-14}, 10^{-13}, 10^{-12}, and 10^{-9} M. (B) Calibration plot of the SWV peak current versus the logarithmic concentration of miRNA. The inset shows the linear range.

with the increase of miRNA concentration from 10 aM to 1 nM, more TWJ2 strands are produced to assist the three-way junction formation and following DHCR. Thus, the SWV peak increases. The detailed relationship between peak intensity and the logarithm of miRNA concentration is depicted in Figure 2B. The relative standard deviation (RSD) of the SWV response is acceptable to promise an analysis with high precision (e.g., 4.9% for 10 fM, 2.9% for 100 fM, 4.2% for 1 nM). A good linear range is established from 10 aM to 100 fM with the regression equation as follows:

$$y = 9.382 + 0.536x \quad (n = 3,\ R^2 = 0.998)$$

in which y stands for the peak current and x is the logarithm of target miRNA. The limit of detection (LOD) of the DHCR based biosensor is calculated to be 7.3 aM (signal-to-noise ratio = 3). It is significantly improved compared with that of the HCR based system (59 aM). We have also compared the analytical performances of this work with recently developed miRNA assays. As listed in Table 1, the sensitivity of this work shows much superiority and the linear range is relatively wide. Meanwhile, the detection time is also acceptable.

Since the target recognition events occur in the solution during the SDA process instead of the common capturing process on the electrode surface, uniform DNA strands for DHCR can be kept when the target sequence is changed, which improves the extensibility of this method for the detection of other targets. In addition, the electrode is supposed to be regenerated by denaturation for repeated use, which may greatly help reduce testing cost. We have then recorded the SWV responses for the detection of miRNA after cycles of regeneration. The reproduced electrode shows nearly blank electrochemical responses. After target triggered SDA and DHCR, the detected peak intensity is also nearly the same with that of the original test, demonstrating the feasibility of electrode regeneration (Figure S4A). We have then studied the

https://dx.doi.org/10.1021/acs.analchem.0c02654
Anal. Chem. 2020, 92, 12026−12032

Table 1. Comparison of the Analytical Performances of Recent miRNA Assays

technique	strategy	time (min)	detection range (M)	LOD (M)	ref
fluorescence	photonic crystal barcodes	240	10^{-9} to 10^{-5}	10^{-9}	25
SERS	miRNA-responsive DNA hydrogel	240	4×10^{-9} to 1.2×10^{-6}	1.1×10^{-10}	26
colorimetry	noncross-linking aggregation of gold nanoparticles	270	10^{-11} to 4×10^{-10}	2.3×10^{-11}	27
fluorescence	rolling circle amplification assisted CRISPR/Cas9 cleavage	190	10^{-12} to 10^{-8}	9×10^{-14}	28
electrochemiluminescence	black phosphorus with perovskite solar cell	120	10^{-13} to 1.5×10^{-8}	4×10^{-14}	29
field-effect transistor	$\pi-\pi$ stacking interaction between DNA and graphene	50	10^{-15} to 10^{-10}	10^{-14}	30
fluorescence	rolling circle amplification molecular network	140	10^{-15} to 10^{-11}	8.6×10^{-16}	31
thermophoretic assay	gold nanoparticles functionalized with fluorophore-labeled DNA sequences	120	1.7×10^{-16} to 1.7×10^{-13}	3.6×10^{-16}	32
electrochemiluminescence	graphitic carbon nitrides functionalized by ABEI	310	10^{-16} to 10^{-12}	4.8×10^{-17}	33
SWV	SDA and DHCR	180	10^{-17} to 10^{-13}	7.3×10^{-18}	this work

reproducibility of this method using different electrodes. Three independent electrodes are modified with TWJ1 with the same protocol. Then, electrochemical measurements are carried out after miRNA triggered reactions with different concentrations, correspondingly. The obtained electrochemical responses using different electrodes are quite close with limited relative standard deviations, verifying good reproducibility of this electrochemical method (Figure S4B).

Investigation of Selectivity and Biological Interference. The selectivity of this method is studied by testing and comparing various other miRNAs and single mismatched sequences with target miRNA. Figure 3A presents that all pure

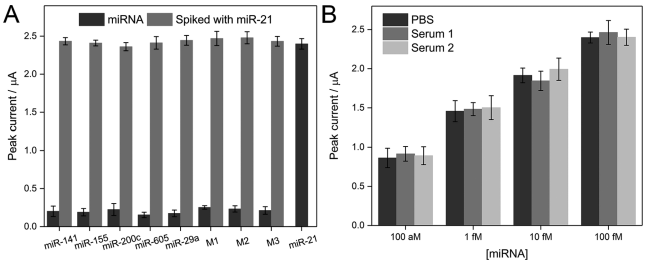

Figure 3. (A) Comparison of peak current for different miRNAs with and without target spiking. (B) Detection of target miRNA in PBS and serum conditions.

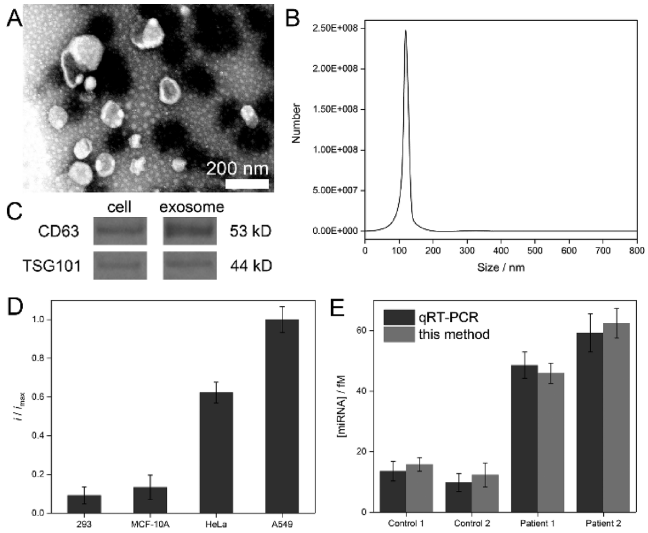

Figure 4. (A) TEM image and (B) nanoparticle tracking analysis of the obtained exosomes. (C) Western blot bands of CD63 and TSG101 in HeLa cells and corresponding exosomes. (D) Comparison of SWV peak currents for the analysis of exosomes from 293, MCF-10A, HeLa, and A549 cells, respectively. (E) Comparison of miRNA detection results of healthy samples and cancer patients' samples by the proposed method and standard qRT-PCR.

interfering miRNAs cannot result in a significant peak current. After being spiked with target miR-21, the peak increases, which is comparable with the performance of pure target. The results confirms that the SWV peak current only shows a positive correlation with target miRNA. The aim of this work is to monitor exosomal miRNA; thus, we have then employed serum samples spiked with different levels of miRNA. The matrix effect is studied by the standard addition method. As shown in Figure 3B, the SWV peaks for testing two serum samples are nearly the same with the PBS performance with the same miRNA level. The matrix effect for the serum 1 sample is from 96.4% to 106.0%. The value for the serum 2 sample is from 100.2% to 104.1%. From the results, it is concluded that miRNA is stable in the biological samples with nearly no interference.

Characterization of Exosomes and Study of Practical Utility. Exosomal miRNA is then directly detected with the proposed approach. Exosomes are first isolated successfully. As shown in the TEM image, a saucer-like morphology is observed, which is the obvious feature of the exosome (Figure 4A). The diameter distribution is then determined to be around 120 nm by nanoparticle tracking analysis (Figure 4B). The size falls in the range of normal exosomes. To make sure the obtained nanoscale vesicle is exosomes, we have performed Western blot experiments to check specific proteins on the surface exosomes. As shown in Figure 4C, the high expression of CD63 and TSG101 can be observed for both cells and exosomes. All these data demonstrate successful isolation of exosomes with high purity.

We have then applied the electrochemical method to analysis exosomal miR-21 derived from different cell lines. Cancer cells are supposed to have higher levels of miR-21 expression. As shown in Figure 4D, the concentrations of miR-21 extracted from cancer cells (HeLa and A549 cells) are much larger than those from normal cells (293, MCF-10A cells), which are in good agreement with the clinical results. The proposed method has the potential to distinguish cancer cells and normal cells selectively according to the electrochemical responses. To further demonstrate the capability of practical utility, we have challenged the method with exosomal miRNAs from clinical serum samples of healthy individuals and breast cancer patients. After measuring the square wave voltammo-

https://dx.doi.org/10.1021/acs.analchem.0c02654
Anal. Chem. 2020, 92, 12026−12032

grams (Figure S5A), miRNA levels are calculated according to the obtained linear equation (inset of Figure 2B). As depicted in Figure 4E, control samples show lower expressions of exosomal miR-21, while patients' serum samples contain much higher concentrations of miR-21. We have also compared the detected results with the qRT-PCR assay. Exosomal total RNA (8 ng per 15 μL reaction) is first reverse transcribed with a TaqMan miRNA reverse transcription kit (Applied Biosystems) and then applied in a qRT-PCR system for measurements. According to the established standard curve (Figure S5B), miRNA levels are calculated and the results corresponding to the same samples are in good accordance with our proposed method. Therefore, it is demonstrated to be a good complement of current liquid biopsy for the exosomal miRNA assay. To achieve clinical application of the proposed method, disposable gold screen printed electrodes can be used to replace traditional gold electrodes. In addition, DNA probes coupled with enzymes and buffers can be integrated in a kit to facilitate standardized manipulation.

CONCLUSION

In summary, we have developed a novel electrochemical method for the detection of exosomal miRNA, taking advantages of SDA and DHCR. The novel design of DHCR not only keeps the high efficacy of hybridization reactions between fuel strands but also results in tight conformation of the DHCR product, which is helpful in shortening the distance between electrochemical species and the electrode interface for the enhancement of the electrochemical response. With the dual signal amplification, the sensitivity is greatly improved and the LOD is as low as 7.3 aM. Extraordinary stability and reproducibility are also demonstrated. This method can be used for the detection of exosomal miRNA not only from cells but also from human serum samples. The results are in excellent agreement with qRT-PCR. Considering all these merits and features, we expect that the proposed method could be a good alternative for exosomal miRNA analysis for POCT diagnosis of cancers in clinical applications.

ASSOCIATED CONTENT

Supporting Information

The Supporting Information is available free of charge at https://pubs.acs.org/doi/10.1021/acs.analchem.0c02654.

Standard free energy calculation, PAGE confirmations of SDA and DHCR, experimental optimizations, regeneration and reproducibility investigations, raw data for real sample assays, and DNA and RNA sequences (PDF)

AUTHOR INFORMATION

Corresponding Author

Peng Miao − *Suzhou Institute of Biomedical Engineering and Technology, Chinese Academy of Sciences, Suzhou, Jiangsu 215163, P. R. China; Department of Chemistry, New York University, New York, New York 10003, United States;* orcid.org/0000-0003-3993-4778; Phone: +86-512-69588279; Email: miaopeng@sibet.ac.cn

Author

Yuguo Tang − *Suzhou Institute of Biomedical Engineering and Technology, Chinese Academy of Sciences, Suzhou, Jiangsu 215163, P. R. China*

Complete contact information is available at: https://pubs.acs.org/10.1021/acs.analchem.0c02654

Author Contributions

All authors have given approval to the final version of the manuscript.

Notes

The authors declare no competing financial interest.

ACKNOWLEDGMENTS

This work was supported by the National Natural Science Foundation of China (Grant no. 81771929) and the Science and Technology Cooperation Project between the Chinese and Australian Governments (Grant no. 2017YFE0132300).

REFERENCES

(1) McGeary, S. E.; Lin, K. S.; Shi, C. Y.; Pham, T. M.; Bisaria, N.; Kelley, G. M.; Bartel, D. P. *Science* **2019**, *366*, eaav1741.
(2) Wang, N.; Zheng, J.; Chen, Z.; Liu, Y.; Dura, B.; Kwak, M.; Xavier-Ferrucio, J.; Lu, Y.-C.; Zhang, M.; Roden, C.; Cheng, J.; Krause, D. S.; Ding, Y.; Fan, R.; Lu, J. *Nat. Commun.* **2019**, *10*, 95.
(3) Peng, Y.; Croce, C. M. *Signal Transduction Targeted Ther.* **2016**, *1*, 15004.
(4) Mulrane, L.; McGee, S. F.; Gallagher, W. M.; O'Connor, D. P. *Cancer Res.* **2013**, *73*, 6554−6562.
(5) Yasui, T.; Yanagida, T.; Ito, S.; Konakade, Y.; Takeshita, D.; Naganawa, T.; Nagashima, K.; Shimada, T.; Kaji, N.; Nakamura, Y.; Thiodorus, I. A.; He, Y.; Rahong, S.; Kanai, M.; Yukawa, H.; Ochiya, T.; Kawai, T.; Baba, Y. *Sci. Adv.* **2017**, *3*, e1701133.
(6) Urabe, F.; Kosaka, N.; Sawa, Y.; Yamamoto, Y.; Ito, K.; Yamamoto, T.; Kimura, T.; Egawa, S.; Ochiya, T. *Sci. Adv.* **2020**, *6*, eaay3051.
(7) El Andaloussi, S.; Mäger, I.; Breakefield, X. O.; Wood, M. J. A. *Nat. Rev. Drug Discovery* **2013**, *12*, 347−357.
(8) Boriachek, K.; Islam, M. N.; Möller, A.; Salomon, C.; Nguyen, N.-T.; Hossain, M. S. A.; Yamauchi, Y.; Shiddiky, M. J. A. *Small* **2018**, *14*, 1702153.
(9) Ren, J.; He, W.; Zheng, L.; Duan, H. *Biomater. Sci.* **2016**, *4*, 910−921.
(10) Théry, C.; Zitvogel, L.; Amigorena, S. *Nat. Rev. Immunol.* **2002**, *2*, 569−579.
(11) Zhang, Y.; Wang, X.-F. *Nat. Cell Biol.* **2015**, *17*, 709−711.
(12) Chen, C.; Zong, S.; Wang, Z.; Lu, J.; Zhu, D.; Zhang, Y.; Zhang, R.; Cui, Y. *Nanoscale* **2018**, *10*, 5154−5162.
(13) Liu, L.; Lu, H.; Shi, R.; Peng, X.-X.; Xiang, Q.; Wang, B.; Wan, Q.-Q.; Sun, Y.; Yang, F.; Zhang, G.-J. *Anal. Chem.* **2019**, *91*, 13198−13205.
(14) Peng, H.; Newbigging, A. M.; Reid, M. S.; Uppal, J. S.; Xu, J.; Zhang, H.; Le, X. C. *Anal. Chem.* **2020**, *92*, 292−308.
(15) Causa, F.; Aliberti, A.; Cusano, A. M.; Battista, E.; Netti, P. A. *J. Am. Chem. Soc.* **2015**, *137*, 1758−1761.
(16) Joshi, G. K.; Deitz-McElyea, S.; Liyanage, T.; Lawrence, K.; Mali, S.; Sardar, R.; Korc, M. *ACS Nano* **2015**, *9*, 11075−11089.
(17) Liu, Q.; Kang, P.-J.; Chen, Z.-P.; Shi, C.-X.; Chen, Y.; Yu, R.-Q. *Chem. Commun.* **2019**, *55*, 14210−14213.
(18) Zhao, Y.; Chen, F.; Zhang, Q.; Zhao, Y.; Zuo, X.; Fan, C. *NPG Asia Mater.* **2014**, *6*, e131.
(19) Yang, D. W.; Tang, Y. G.; Miao, P. *TrAC, Trends Anal. Chem.* **2017**, *94*, 1−13.
(20) Evanko, D. *Nat. Methods* **2004**, *1*, 186.
(21) Ge, Z.; Lin, M.; Wang, P.; Pei, H.; Yan, J.; Shi, J.; Huang, Q.; He, D.; Fan, C.; Zuo, X. *Anal. Chem.* **2014**, *86*, 2124−2130.
(22) Liu, G.; Chai, H.; Tang, Y.; Miao, P. *Chem. Commun.* **2020**, *56*, 1175−1178.
(23) Yu, L.; He, P.; Xu, Y.; Kou, X.; Yu, Z.; Xie, X.; Miao, P. *Sens. Actuators, B* **2020**, *313*, 128015.
(24) Jiang, Y.; Miao, P. *Research* **2020**, *2020*, 1091605.

(25) Wei, X.; Bian, F.; Cai, X.; Wang, Y.; Cai, L.; Yang, J.; Zhu, Y.; Zhao, Y. *Anal. Chem.* **2020**, *92*, 6121−6127.
(26) Si, Y.; Xu, L.; Wang, N.; Zheng, J.; Yang, R.; Li, J. *Anal. Chem.* **2020**, *92*, 2649−2655.
(27) Ma, X.; Chen, X.; Tang, Y.; Yan, R.; Miao, P. *ACS Appl. Mater. Interfaces* **2019**, *11*, 41157−41164.
(28) Wang, R.; Zhao, X.; Chen, X.; Qiu, X.; Qing, G.; Zhang, H.; Zhang, L.; Hu, X.; He, Z.; Zhong, D.; Wang, Y.; Luo, Y. *Anal. Chem.* **2020**, *92*, 2176−2185.
(29) Gao, C.; Yu, H.; Wang, Y.; Liu, D.; Wen, T.; Zhang, L.; Ge, S.; Yu, J. *Anal. Chem.* **2020**, *92*, 6822−6826.
(30) Gao, J.; Gao, Y.; Han, Y.; Pang, J.; Wang, C.; Wang, Y.; Liu, H.; Zhang, Y.; Han, L. *ACS Appl. Electron. Mater.* **2020**, *2*, 1090−1098.
(31) Li, D.; Zhang, T.; Yang, F.; Yuan, R.; Xiang, Y. *Anal. Chem.* **2020**, *92*, 2074−2079.
(32) Zhao, J.; Liu, C.; Li, Y.; Ma, Y.; Deng, J.; Li, L.; Sun, J. *J. Am. Chem. Soc.* **2020**, *142*, 4996−5001.
(33) Wang, J.; Haghighatbin, M. A.; Shen, W.; Mi, L.; Cui, H. *Anal. Chem.* **2020**, *92*, 7062−7070.

https://dx.doi.org/10.1021/acs.analchem.0c02654
Anal. Chem. 2020, 92, 12026−12032